

# Development of Magnesium Anode-Based Transient Primary Batteries

Jazer Jose H. Togonon,<sup>[a, b]</sup> Eugene A. Esparcia, Jr.,<sup>[a]</sup> Julie Anne D. del Rosario,<sup>[a, b]</sup> and Joey D. Ocon<sup>\*[a, b]</sup>

Biodegradable primary batteries, also known as transient batteries, are essential to realize autonomous biodegradable electronic devices with high performance and advanced functionality. In this work, magnesium, copper, iron, and zinc – metals that exist as trace elements in the human body – were tested as materials for biomedical transient electronic devices. Different full cell combinations of Mg and X (where X = Cu, Fe, and Zn and the anodized form of the metals) with phosphate buffered saline (PBS) as electrolyte were studied. To form the cathodes, metal foils were anodized galvanostatically at a current density of  $2.0 \text{ mA cm}^{-2}$  for 30 mins. Electrochemical measurements were then conducted for each electrode combination to evaluate full cell battery performance. Results showed that the Mg–Cu<sub>anodized</sub> chemistry has the highest power density at  $0.99 \text{ mW/cm}^2$ . Nominal operating voltages of 1.26 V for the first 0.50 h and 0.63 V for the next 3.7 h were observed for Mg–Cu<sub>anodized</sub> which was discharged at a current density of  $0.70 \text{ mA cm}^{-2}$ . Among the materials tested, Mg–Cu<sub>anodized</sub> exhibited the best discharge performance with an average specific capacity of  $2.94 \text{ mAh cm}^{-2}$ , which is comparable to previous reports on transient batteries.

## 1. Introduction

There has been an emergence of transient electronics in recent years, particularly for biomedical and environmental sensing/monitoring applications. These devices are capable of performing a variety of functions and are triggered by


external mechanisms such as exposure to light, heat, or aqueous solvent.<sup>[1]</sup> The key attribute of these devices is their ability to physically disappear, entirely or in part, in a controlled manner after a typically short and well-defined period of stable operation when transiency is triggered.<sup>[1–3]</sup> Currently, these devices use an external power source such as inducting coils from a very close distance.<sup>[1,4]</sup> For some implantable medical devices (IMD), instead of having a bulky external power source, the device is limited to either wireless powering or electrically passive designs.<sup>[3]</sup> Through the utilization of on-board transient power supplies, permanent IMDs, specifically for transient use, can potentially be converted into temporary IMDs. Apart from having extended functionalities, the need for post-operative and revision surgery procedures to recover the device are also eliminated. Risks associated with the procedure such as bacterial infections are also avoided. In addition, the use of temporary implants which could eliminate the occurrence of chronic inflammation and other long-term effects associated with permanent implants is more economically beneficial.


In the field of environmental sensing and monitoring, the need for transient devices mainly stems from the need for electronic devices to address environmental challenges. Transient technology enables electronics to be zero-waste given that these green electronics can degrade naturally into the surrounding after a certain period of operation.<sup>[5]</sup> The degradability of environmental sensors eliminates the waste streams associated with recycling and disposal, and the practical difficulties in device collection and recovery.<sup>[6]</sup> For this application, transient batteries are required to be environmentally friendly.

Recent studies are looking into biodegradable battery systems that can partially or fully degrade its components when the device has served its intended function.<sup>[1–7]</sup> Design constraints of such batteries, however, include compactness, energy content, performance, shelf-life, biodegradability, and biocompatibility.<sup>[3]</sup> Suitable battery chemistry should satisfy the energy and power requirements but should degrade into non-toxic products after serving its discharge lifetime. For permanent IMDs and environmental sensors, energy requirements typically ranges from units of  $\mu\text{W}$  to  $\text{mW}$  depending on the application.<sup>[8]</sup> For example, wireless endoscopes relying on ingestible sensors require power of up to  $10 \text{ mW}$ .<sup>[8]</sup> Currently, there are significant challenges in developing on-board power generation for transient devices. The main hurdle is the lack of soluble biocompatible materials.<sup>[1]</sup> A number of research have focused on magnesium (Mg) as the

[a] J. J. H. Togonon, E. A. Esparcia, Jr., Prof. J. A. D. del Rosario, Prof. J. D. Ocon  
Laboratory of Electrochemical Engineering (LEE)  
Department of Chemical Engineering  
College of Engineering  
University of the Philippines Diliman  
Quezon City 1101 (Philippines)  
E-mail: jdocon@up.edu.ph

[b] J. J. H. Togonon, Prof. J. A. D. del Rosario, Prof. J. D. Ocon  
Energy Engineering Program  
College of Engineering  
University of the Philippines Diliman  
Quezon City 1101 (Philippines)

 Supporting information for this article is available on the WWW under <https://doi.org/10.1002/open.202000168>

 © 2021 The Authors. Published by Wiley-VCH GmbH. This is an open access article under the terms of the Creative Commons Attribution Non-Commercial NoDerivs License, which permits use and distribution in any medium, provided the original work is properly cited, the use is non-commercial and no modifications or adaptations are made.

anode material in the development of transient batteries because of its high energy density, long shelf-life, and desirable biocompatibility.<sup>[2,3,7,9]</sup> In addition to the anode material, the selection for a compatible cathode is also important in order to fully evaluate the performance of a full cell. Cathode materials used in previous researches include iron (Fe), tungsten (W), molybdenum (Mo),<sup>[2]</sup> and  $\lambda$ -manganese oxide ( $\lambda$ -MnO<sub>2</sub>).<sup>[4]</sup>

Other metals including copper (Cu) and zinc (Zn), which appear in trace amounts in the human body and play an important role in several biocellular and physiological processes have also been studied for biomedical and environmental applications.<sup>[10–15]</sup> It is also worth noting that these metals may cause adverse effects at high concentrations and each has finite allowable limits in different biological systems.<sup>[11,14,15]</sup> Metal oxide nanomaterials such as Cu oxide,<sup>[16]</sup> Fe oxide,<sup>[17]</sup> and Zn oxide<sup>[18]</sup> are also becoming increasingly important as one of the newest class of materials used in the drug industry and other health related applications. Their unique structure, catalytic properties, high surface area, good mechanical stability and biocompatibility attracted considerable interest in the field of biomedical therapeutics, bio-imaging, and bio-sensing.<sup>[19]</sup> Electrolyte selection is another crucial factor in the performance of transient batteries. The choice of electrolyte will ultimately depend on the application of the transient device. For IMD application, the usual electrolyte used in research studies is phosphate buffered saline solution (PBS) as it is a suitable analog for in vitro studies.<sup>[2–4]</sup>

The development of biodegradable energy sources supports the design of autonomous electronics with greater functionality and permits sensing and actuation over well-defined time periods. Thus, in this work, different combinations of transient primary battery chemistries using Cu, Fe, and Zn with their anodized forms as cathode, Mg as the anode, and PBS as the battery electrolyte were evaluated. The pertinent electrochemical performances such as discharge performance and stability of the battery combination were also elucidated.

## 2. Results and Discussion

### 2.1. Anodization of Electrodes

The unique idea of this work is testing both metal and its metal oxide, which are synthesized via anodization,<sup>[20]</sup> as the positive electrode of the Mg-based transient primary battery. During anodization, a positive current is continuously applied to form an oxide layer on the surface of the metal. Figure 1 shows the SEM images of the surface of Cu, Fe, and Zn before and after the anodization process. The formation of the oxide layer was observed after anodization of metals with different morphology which are then confirmed using XRD.

Figure 2 shows the XRD pattern of the metals before and after anodization. Thorn-like microstructures were formed on the surface of the Cu foil (Figure 1A and 1B). Observable XRD peaks (Figure 2A) correspond to formation of copper oxides (CuO and Cu<sub>2</sub>O) and copper hydroxide (Cu(OH)<sub>2</sub>). On

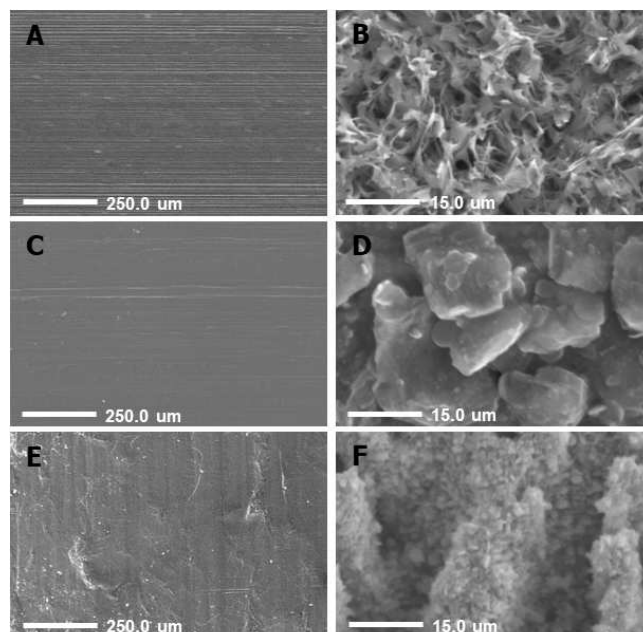


**Figure 1.** SEM images of (A) before and (B) after the anodization of copper; (C) before and (D) after the anodization of iron; and (E) before and (F) after the anodization of zinc.

the other hand, two new peaks at 19.3° and 30.0° (Figure 2B) were observed from the surface of the Fe foil which probably corresponds to prominent peaks of Fe(OH)<sub>2</sub> and  $\gamma$ -Fe<sub>2</sub>O<sub>3</sub>. The material composition is highly likely considering that OH<sup>-</sup> is present in the electrolyte and  $\gamma$ -Fe<sub>2</sub>O<sub>3</sub> is readily observed in Fe anodization process. The absence of other peaks and presence of high background noise in the XRD pattern of iron-based materials can be attributed to adsorption and fluorescence of Fe under X-ray radiation using Cu as radiation source.<sup>[21]</sup> Further confirmation of the iron-based material composition and phases is recommended using other X-ray radiation sources. Non-uniform formation can be observed on the SEM results (Figure 1C and 1D) possibly due to the insufficient current applied during anodization process. Conversely, the formation of wurtzite ZnO (36.3°) and  $\epsilon$ -Zn(OH)<sub>2</sub> (20.2°, 28.7°) (Figure 2C) were observed on the Zn foil (Figure 1F). Formation of zinc hydroxychloride (Zn<sub>5</sub>(OH)<sub>8</sub>Cl<sub>2</sub>·H<sub>2</sub>O) was also observed (~11.6°)<sup>[22]</sup> which probably comes from the residue of Cl<sup>-</sup> retained after the initial cleaning of Zn foil with HCl (see supplementary information).

### 2.2. Electrochemical Properties

Figure 3 shows the I–V characteristic curves of the different battery chemistries. Theoretically, the standard reduction potentials for metals are used to estimate the cell voltages of different battery combinations. The cell voltage is the difference between the cathode and the anode reduction potentials. The material which is more electronegative will act as the anode

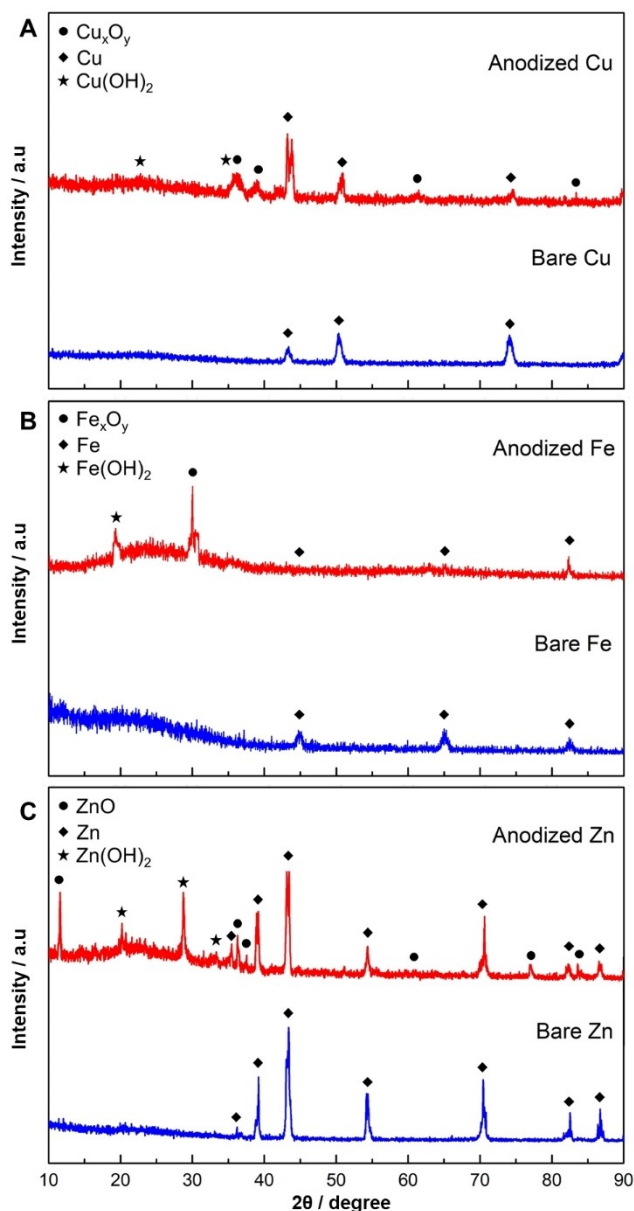


Figure 2. XRD pattern of (A) bare and anodized Cu, (B) bare and anodized Fe, (C) bare and anodized Zn

and the paired material will act as the cathode. For the case of Mg–Cu full cell, the potential difference between the two electrodes should be 2.71 V.<sup>[11]</sup> However in this case, several works<sup>[2,3]</sup> suggest that either oxygen reduction reaction or hydrogen evolution reaction occur rather than cathode reduction.

The main electrochemical reactions of the battery are as follows:<sup>[13]</sup>

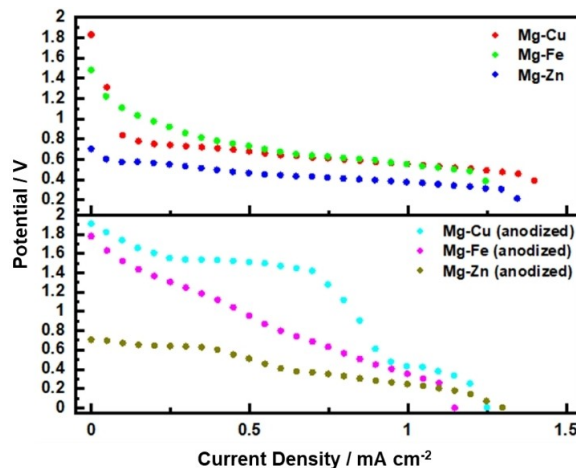
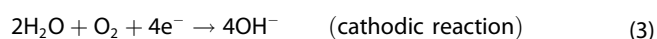
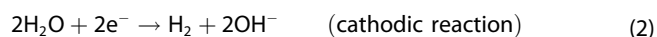
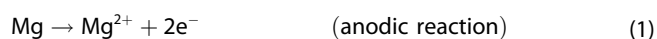
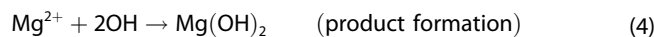


Figure 3. Current-Voltage (IV) characteristic curve of different battery combinations



At discharge current of  $0.50 \text{ mA cm}^{-2}$ , the operating voltage of the Mg–Cu cell is around 0.70 V–0.75 V, the approximately 2.0 V difference from theoretical is likely to be the result of polarization effects and relatively high discharge rate applied. These results are expected for all battery chemistries, especially when solution conductivity of the electrolyte is not high.

### 2.3. Discharge Testing

The galvanostatic discharge test was performed for all electrode combinations in order to evaluate the capacity and kinetic behavior of the cells (Figure 4). The fluctuations in the

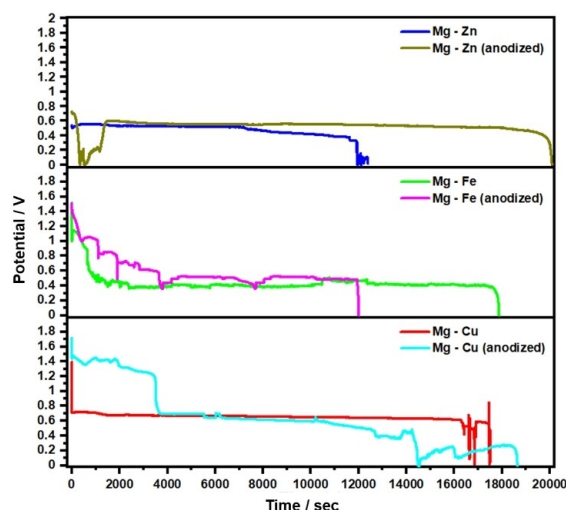


Figure 4. Discharge profile of the different electrode combination using pure metal and metal oxides cathodes at  $0.50 \text{ mA cm}^{-2}$  applied current density; and discharge profile of Mg–Cu oxide (C) at  $0.70 \text{ mA cm}^{-2}$  applied current density.

discharge profile are highly associated with electrode interaction to the phosphate buffer solution (PBS). Aside from the formation of  $\text{Mg}(\text{OH})_2$  during discharge process, the competing effect of chlorine and phosphate ions in PBS to the corrosion rates affect the discharge profile of the battery cell.<sup>[3]</sup> Moreover, the discharge process highly depends on the amount of the active material, Mg, which is consumed after some time. This means that the morphology of Mg during discharge undergoes pitting corrosion which could also affect the performance causing some fluctuations in the voltage reading.<sup>[14]</sup>

On the cathode side, the formation of hydrogen gas occurs during the discharge process. Added fluctuations in the discharge profile can be due to the hydrogen gas adherence to the cathode surface, which intermittently reduces the reaction area.<sup>[2]</sup> In addition, the hydrodynamics of the system associated with the hydrogen gas formation can compromise the structure of the metal, therefore potentially ending the discharge process prematurely. The combinations that use metal cathodes have relatively more stable discharge outputs than the metal oxide cathodes. This observed discharge characteristics is possibly due to the pristine surface of the metal foils compared to the morphologically changed surfaces of the metal oxides.

Results show in general that anodized metal cathodes have more complex curves due to the interaction of metal oxides and subsequently of its metal form with the solution. For instance, zinc oxide drops to 0 V before having a very stable profile due to very low electronic conductivity of zinc oxide.<sup>[3]</sup> It is suggested that the oxide on the surfaces of the metal became the sites for the hydrogen evolution reaction. The prolonged application of constant current subsequently stripped and removed the oxide on the surfaces of the metal. The zinc oxide is removed from the electrode, exposing the zinc metal. In the case of  $\text{Mg}-\text{Cu}_{\text{anodized}}$ , the stripping and removal of the oxide on the surface is readily observed and can be seen in the discharge profile as well.

Among the battery combinations studied here,  $\text{Mg}-\text{Cu}_{\text{anodized}}$  obtained the highest discharge voltage when a current density of  $0.50 \text{ mA cm}^{-2}$  was applied. For almost 1 h of discharge operation, an average discharge voltage of 1.40 V was recorded. When the battery was discharged further, the discharge voltage falls and maintained around 0.60 V for about 3 h more, after which unsteady reading was observed. The result of  $\text{Mg}-\text{Zn}_{\text{anodized}}$  battery during discharge showed a more stable output voltage among all battery chemistry. This may give us the idea that redox reaction present on the surface of the material is most suitable and compatible with the surface of ZnO.

Further investigation was performed using the anodized Cu as the cathode material and was discharged at a current density of  $\sim 0.70 \text{ mA cm}^{-2}$  as shown in Figure 5. It is important to note that the current density of  $0.70 \text{ mA cm}^{-2}$  was only applied to  $\text{Mg}-\text{Cu}_{\text{anodized}}$  combination because it is the determined discharge current where the peak power density is achieved based on the I-V characteristic curve. The case for  $\text{Mg}-\text{Cu}_{\text{anodized}}$  showed two (2) plateaus suggesting that the

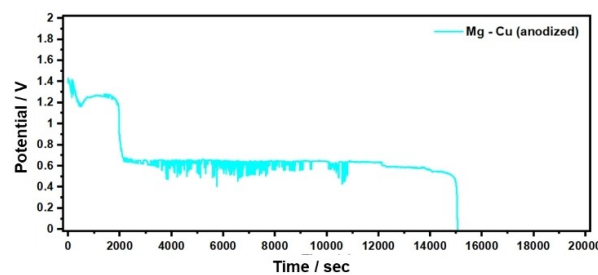


Figure 5. Discharge profile of  $\text{Mg}-\text{Cu}$  oxide (C) at  $0.70 \text{ mA cm}^{-2}$  applied current density.

present Cu oxide interacts to the system first and then bare Cu will interact after the removal of the oxide layer. This trend is similar and can also be observed when the discharge current applied was  $0.5 \text{ mA cm}^{-2}$ . It was also observed that when  $\text{Mg}-\text{Cu}_{\text{anodized}}$  was discharged at higher current density, the life of the battery is shorter. The nominal operating voltages of  $\text{Mg}-\text{Cu}_{\text{anodized}}$  battery was recorded at 1.26 V for the first 0.50 h and 0.63 V for the next 3.7 h giving an average specific capacity of  $2.94 \text{ mAh cm}^{-2}$ .

### 3. Conclusion

This work investigated the electrochemical performance of six different electrode combinations ( $\text{Mg}-\text{Cu}$ ,  $\text{Mg}-\text{Fe}$ ,  $\text{Mg}-\text{Zn}$ ,  $\text{Mg}-\text{Cu}_{\text{anodized}}$ ,  $\text{Mg}-\text{Fe}_{\text{anodized}}$ , and  $\text{Mg}-\text{Zn}_{\text{anodized}}$ ) in 1X PBS aqueous solution as electrolyte. The methodical examination of different full cell combinations revealed the critical chemical reactions and phenomena governing the performance of Mg-based biodegradable batteries. Two possible reaction mechanisms are present at the cathode side which is coupled with the oxidation reaction at the anode side of the battery. The reactions at the cathode side can either be the reduction of oxygen or the evolution of hydrogen and is dependent on the applied discharge current of the battery. The life of the battery is crucially determined and highly reliant on the amount of the material in the anode side which is also considered as the active material in the study. The cells operate at different voltage ranges which are sufficient in powering small devices. High losses in the nominal voltage were observed which may be mostly due to the passivating layer of products formed on the surface of the electrodes.

The facile anodization procedure<sup>[20]</sup> that was implemented in the study was able to provide sufficient oxide layer for the Cu and Zn cathode materials of the biodegradable primary battery. It should also be noted that metal hydroxides were also formed on the surface of the metal which may likely to have an effect to the overall performance of the batteries. For the first time, we were able to elucidate the added effect on the performance of the battery with anodized metals as cathode in contrast with bare and pristine metals. The additional oxide layer may have promoted supplemental sites for hydrogen evolution reaction which subsequently increased the operating voltages of the battery. It is recommended that the effect of the thickness and

morphology of the metal oxide should be explored to fully understand the mechanisms present.

Additionally, different approaches on oxide synthesis may be evaluated and tested to form a more suitable oxide morphology for this specific application. It is suggested to validate the actual biocompatibility of the oxide layer as this may promote toxic reactions in the host if deployed. The amount of formed products in the electrochemical reaction of the biodegradable metals should be taken into serious consideration such that it is below the allowable limit of in the human body.<sup>[14]</sup>

## Experimental Section

### General

Mg metal (Goodfellow Cambridge Ltd., 99.99%, 25 mm×25 mm), Zn metal (99.99%, 50 mm×50 mm), Fe metal (99.99%, 50 mm×50 mm), and Cu metal (99.99%, 50 mm×50 mm) were used as electrode material. Metal foils were cut to strips (5 mm×25 mm) for testing. After cutting, the strips were cleaned using reasonable amount of 0.01 M HCl (Sigma-Aldrich) in order to remove native oxides present on the metal surface. Phosphate buffered saline solution (PBS) (Sigma-Aldrich, 1X) was later used as electrolyte solution for electrochemical measurements.

### Anodization of Metals

Cu, Fe, and Zn were galvanostatically discharged separately using a potentiostat (Metrohm Autolab PGSTAT302 N). A three-electrode configuration was setup with the metal sample, saturated silver/silver chloride (Ag/AgCl), and a platinum (Pt) plate as the working electrode, reference electrode, and counter electrode, respectively. A current density of 2.0 mAcm<sup>-2</sup> was applied in 2.0 M KOH solution for 30 mins to grow the oxide layer on the surface of the metal foil.

### Material Characterization

Scanning electron microscope (Hitachi SEM S-3400) was used to determine the surface morphology of the metal oxide. The films were first subjected to ion sputtering (Hitachi Ion Sputter E-1045) in Pd/Au to allow better conductivity and images for surface microscopy. The samples were then mounted on the SEM holder. Different images at different sites with varying magnification were taken to obtain the surface morphology and to validate the uniformity of the surface. X-ray diffraction (Shimadzu Maxima XRD-7000) was used to identify the phase of the crystalline material. The anodized metal foils were subjected to a full scan X-ray diffraction analysis set at 10° to 90°, 2 $\theta$  angle. X-ray beams were generated from a Cu-K $\alpha$  radiation source (40 kV; 30 mA) with wavelength of 1.54 Å. The resolution for the analysis was set at 0.02°, with scan speed maintained at 2° per minute. The detection limit is 5% and strongly dependent on the crystallinity. These surface characterization techniques were done to confirm the presence of the oxide layer synthesized during the anodization step of the study.

## Electrochemical Measurements of the Different Electrode Combinations

Six different electrode combinations (Mg–Cu, Mg–Fe, Mg–Zn, Mg–Cu<sub>anodized</sub>, Mg–Fe<sub>anodized</sub>, and Mg–Zn<sub>anodized</sub>) were evaluated by performing galvanostatic discharge tests in a two-electrode cell configuration using a potentiostat (Metrohm Autolab PGSTAT302N). The current-voltage (I–V) characteristics of each electrode combinations and their corresponding power curves were evaluated in order to select the best combination. The metal foils were cut and a contact area of 75 mm<sup>2</sup> (15 mm×5 mm) was used. Constant current densities ranging from 0.05 mAcm<sup>-2</sup> to 1 mAcm<sup>-2</sup> (with 0.05 mAcm<sup>-2</sup> increment for 300 seconds) was applied in 1X PBS solution as electrolyte. The discharge curve of each configuration was evaluated to understand their performance and behavior with degradation during operation. All battery chemistry combinations were discharged at 0.50 mAcm<sup>-2</sup>. For the battery combination that provided the highest power density, the said combination was discharged at the optimum current density.

## Acknowledgements

The authors would like to acknowledge the financial support from the Engineering Research and Development for Technology (ERDT) Program of the Department of Science and Technology (DOST). J.D. Ocon is grateful for the support of the UP Office of Vice Chancellor for Research and Development – PhD Incentive Award, and the Commission on Higher Education – Philippine California Advanced Research Institutes (CHED-PCARI) GREEN POWER PROGRAM IIID-2015-09.

## Conflict of Interest

The authors declare no conflict of interest.

**Keywords:** anodization process · magnesium · metal oxide cathodes · transient batteries

- [1] Y. Chen, R. Jamshidi, K. White, S. Çinar, E. Gallegos, N. Hashemi, R. Montazami, *J. Polym. Sci. Part B Polym. Phys.* **2016**, *54*, 2021.
- [2] L. Yin, X. Huang, H. Xu, Y. Zhang, J. Lam, J. Cheng, J. A. Rogers, *Adv. Mater.* **2014**, *26*, 3879.
- [3] M. Tsang, A. Armutlulu, A. W. Martinez, S. A. B. Allen, M. G. Allen, *Microsystems Nanoeng.* **2015**, *1*, 15024.
- [4] Y. J. Kim, W. Wu, S.-E. Chun, J. F. Whitacre, C. J. Bettinger, *Proc. Natl. Acad. Sci. USA* **2013**, *110*, 20912.
- [5] K. K. Fu, Z. Wang, J. Dai, M. Carter, L. Hu, *Chem. Mater.* **2016**, *28*, 3527.
- [6] S. W. Hwang, J. K. Song, X. Huang, H. Cheng, S. K. Kang, B. H. Kim, J. H. Kim, S. Yu, Y. Huang, J. A. Rogers, *Adv. Mater.* **2014**, *26*, 3905.
- [7] M. Tsang, A. Armutlulu, A. Martinez, F. Herrault, S. A. B. Allen, M. G. Allen, In *Proceedings of the IEEE International Conference on Micro Electro Mechanical Systems (MEMS)*, **2014**; pp. 358–361.
- [8] S. Stauss, I. Honma, *Bull. Chem. Soc. Jpn.* **2018**, *91*, 492.
- [9] M. Tsang, A. Armutlulu, F. Herrault, R. H. Shafer, S. A. B. Allen, M. G. Allen, *J. Microelectromechanical Syst.* **2014**, *23*, 1281.
- [10] M. M. O. Peña, J. Lee, D. J. Thiele, *J. Nutr.* **1999**, *129*, 1251.
- [11] M. Bost, S. Houdart, M. Oberli, E. Kalonji, J. F. Huneau, I. Margaritis, *J. Trace Elem. Med. Biol.* **2016**, *35*, 107.
- [12] D. Mitra, E. T. Kang, K. G. Neoh, *ACS Appl. Mater. Interfaces* **2020**, *12*, 21159.

- [13] Y. Yun, Z. Dong, N. Lee, Y. Liu, D. Xue, X. Guo, J. Kuhlmann, A. Doepke, H. B. Halsall, W. Heineman, S. Sundaramurthy, M. J. Schulz, Z. Yin, V. Shanov, D. Hurd, P. Nagy, W. Li, C. Fox, *Mater. Today* **2009**, *12*, 22.
- [14] Y. F. Zheng, X. N. Gu, F. Witte, *Mater. Sci. Eng. R* **2014**, *77*, 1.
- [15] H. Li, Y. Zheng, L. Qin, *Prog. Nat. Sci. Mater. Int.* **2014**, *24*, 414–422.
- [16] N. Verma, N. Kumar, *ACS Biomater. Sci. Eng.* **2019**, *5*, 1170.
- [17] P. Sangaiya, R. Jayaprakash, *J. Supercond. Nov. Magn.* **2018**, *31*, 3397.
- [18] Y. Zhang, T. R. Nayak, H. Hong, W. Cai, *Curr. Mol. Med.* **2013**, *13*, 1633.
- [19] S. Andreescu, M. Ornatska, J. S. Erlichman, A. Estevez, J. C. Leiter, *Fine Part. Med. Pharm.* **2012**, *9781461403*.
- [20] N. Muralidharan, A. Westover, H. Sun, N. Galio, R. Carter, A. Cohn, L. Oakes, C. Pint, *ACS Energy Lett.* **2016**, *1*, 1034.
- [21] Y. M. Mos, A. C. Vermeulen, C. J. N. Buisman, J. Weijma, *Geomicrobiol. J.* **2018**, *35*, 511.
- [22] F. C. Hawthorne, E. Sokolova, *Can. Mineral.* **2002**, *40*, 939.

---

Manuscript received: June 4, 2020

Revised manuscript received: February 3, 2021